Minerals Engineering 232 (2025) 109595

Contents lists available at ScienceDirect

Minerals Engineering

journal homepage: www.elsevier.com/locate/mineng

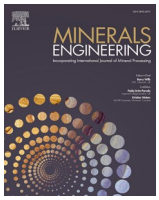

Kinetics analysis and $Cr^{(6+)}$-free reaction mechanism of the alkali reduction of South African chromite ores for Cr_2O_3 extraction

S. Sanchez-Segado [a,*], L. Escudero-Castejón [b], A. Jha [b,*]

[a] Universidad Politécnica de Cartagena, Departamento de Ingeniería Química y Ambiental, Campus Muralla del Mar, C/Doctor Fleming, s/n, 30202 Cartagena España, Spain
[b] School of Chemical and Process Engineering, University of Leeds, Leeds LS2 9JT, UK

ARTICLE INFO

Keywords:
Chromite ore
Chromium
Reduction Roasting
Kinetics
Reaction mechanism

ABSTRACT

The generation of the Cr^{6+}-ion containing chromite ore processing residue (COPR) from the oxidative alkali roasting is still a significant environmental challenge faced by the chromium chemicals industry. The oxidative roasting of Cr_2O_3 in the presence of alkali yields water-soluble sodium chromate (Na_2CrO_4), traces of which remains trapped within the interconnected porous structures of COPR in spite of multiple leaching and washing stages. In this article, we present an alternative route and have investigated the kinetics of a novel reductive alkali roasting reaction which eliminates the formation of Cr^{6+} state by maintaining Cr^{3+}-ion as sodium chromite ($NaCrO_2$), which is insoluble in water. The reaction kinetics of reductive alkali roasting of South African chromite ore were investigated in an inert atmosphere in the temperature range of 850 °C to 1050 °C. The effects of process parameters, namely, time, temperature, and alkali-to-carbon ratio, on the reducibility of South African chromite ore were investigated. It was observed that the highest reducibility of South African chromite was observed for a reactant mixture in a weight ratio of chromite: Na_2CO_3:C = 1:1:0.2 which was reduced at 1050 °C for 2.5 h. Using the isothermal kinetic data, the activation energy analysis for the alkali reduction of chromite was carried out which confirms a diffusion-controlled process, as described by the Ginstling and Brounstein model. The derived value apparent activation energy (E_a) was found to be 206.0 ± 0.8 kJ mol^{-1} per mole of Cr_2O_3. Based on the apparent diffusion model, the phase changes during the alkali reduction reaction are explained.

1. Introduction

Chromium oxide is found in the earth crust as chromite ore which can be expressed with the normal spinel crystal structure [(M_1), $\{M_2\}_2]_3O_4$ formula. In the chromite mineral, the distribution of general cationic site distribution is represented by four cations shown in the formula unit: [(Fe, Mg),{Cr, Al, Fe}$_2]_3O_4$ in which the divalent ions occupy the tetrahedron sites whereas the trivalent ions occupy the octahedron sites, due to the difference in the site preference energy (Escudero-Castejon et al., 2016; Sergio Sanchez-Segado et al., 2015a; Tathavakar et al., 2005). The chromite ore is the natural resource for extracting chromium oxide for metals and alloy production (Cunat, 2004). Global economic growth in the last few decades has led to an increasing demand for stainless steel and other chromium-containing high-temperature alloys, as shown in Fig. 1a and 1b. According to the global resources data, the amount of shipping-grade chromite is more than 12 billion tonnes, and the world mine production of marketable chromite ore is 44 million of metric tons; with South Africa, Turkey and Kazakhstan being the main producers with 39 %, 23 % and 15 % of the share, respectively (Mineral commodity summaries 2024, 2024). The global stainless steel production has increased from just under 24 million of metric tonnes in 2010 to 51 million in 2020.

The most important application of chromite is in the production of high-grade ferro-chromium, which is used in the metallurgical industry for manufacturing of stainless steels and chromium-containing metal alloys (Papp, 1994). The ferro-chromium alloy is produced by smelting of chromite ore in reducing atmosphere in a submerged arc furnace with coke at temperatures above 1600 °C which consumes from 3000 to 4200 kWh of energy per tonne (Ramakrishna et al., 2015). In the submerged arc melting, the temperature and oxygen potential are controlled carefully to avoid the formation of complex carbides and loss of sub-oxide of chromium (CrO) in the gas phase. The control of soluble carbon in the

* Corresponding authors.
E-mail addresses: sergio.segado@upct.es (S. Sanchez-Segado), A.Jha@leeds.ac.uk (A. Jha).

https://doi.org/10.1016/j.mineng.2025.109595
Received 8 October 2024; Received in revised form 6 June 2025; Accepted 4 July 2025
Available online 8 July 2025

liquid and solidified Fe-Cr alloy is essential for minimizing the precipitation of complex binary and ternary carbides (Benz et al., 1974; Kundrat et al., 1984). The control of carbon is achieved in a two-step process by rapid melting in the arc furnace followed by optimal deoxidation by forming CO gas using iron oxide. The final carbon concentration is critical for determining the applications in the production of ferritic and austenitic stainless steel and super alloys. The unoptimized carbon concentration in Fe-Cr alloy leads to the formation of surface defects in the sheet products. Besides the control of carbon during electric arc melting, the concentration of silicon is also important, as the presence of silicon increases the chemical potential for the formation of brittle silicide phases (Azimi and Shamanian, 2010) which like carbides introduce surface defects during sheet rolling process. For these reasons, controlling silicon and carbon in ferrochrome is critical. Furthermore, as the austenitic and ferritic stainless steels are also used for a range of high temperature and oxidative corrosion resistance applications, during arc melting, the concentrations of sulphur and phosphorus are also controlled to a level below 0.02 % w/w, because following the ferrochrome alloy making step it is only carbon which is reduced to below 0.08 % w/w during the argon-oxygen decarburization (AOD) process (Holappa, 2014). With the aim of decreasing the high energy consumption of the smelting process, the partial solid-state reduction of chromite was demonstrated in a rotary kiln at temperatures between 1200 °C to 1400 °C, before smelting (Chakraborty et al., 2005; Ranganathan et al., 2011). However, this process has its own limitations such as the high temperature required and the slow kinetics of chromium reduction process (Hazar-Yoruç, 2007).

Various oxidative processes such as the soda-ash roasting, acid leaching, alkali leaching and alkali fusion, have been developed for the processing of chromite ores in order to produce sodium chromate (Na_2CrO_4), which is the primary product used for the manufacturing of a wide range of chromium chemicals; because of economic and technical reasons, just soda-ash roasting has been used worldwide on a commercial scale, either in a rotary kiln or in a rotary hearth furnace (Antony et al., 2001; Geveci et al., 2002; Sun et al., 2007; Tathavadkar et al., 2003; Tinjum et al., 2008; Yildiz and Sengil, 2004). Le Chatelier, in the 19th century, first applied alkali roasting in oxidising conditions for the extraction of sodium chromate from chromite ores (Jha, 2011). This discovery set the basis for the industrial process which is still practiced today. The application of the alkali roasting process for the extraction of different metal oxides, such as Ti, Nb, Ta, rare earths, Al or V, from complex minerals has also been investigated with satisfactory results (Borra et al., 2017; Ghambi et al., 2021; Lahiri and Jha, 2007; Sanchez-Segado et al., 2022, Sanchez-Segado et al., 2017, 2014). The alkali roasting of chromite in the presence of oxygen or air is based on the oxidation of Cr^{3+} to Cr^{6+} ionic state in the mineral in the temperature range of 1000–1200 °C, which leads to formation of water-soluble chromates (Parirenyatwa et al., 2016; S. Sanchez-Segado et al., 2015a). The roasted material is subsequently leached with water to selectively solubilise sodium chromate. The remaining insoluble solid, known as the chromite ore processing residue (COPR), mainly contains iron oxide, magnesium oxide, insoluble silicates and unreacted chromite. The topochemical progression of oxidation reaction leaves unreacted and porous chromite core particulates, which retains the water-soluble sodium chromate (Cr^{6+} ions) and due to limited diffusivity through pores, complete removal of residual Cr^{6+}-ions (>0.1 wt%) remains challenging and consequently, the COPR remains a waste as carcinogen and ecological hazard with only option of disposal by landfilling. Hexavalent chromium is known to be a hazardous chemical, for all living beings because it is classed as carcinogenic, mutagenic, and teratogenic; implication of such a profound toxicity might spread by air, water, and land. For this reason, worldwide COPR waste is contained and capped inside designated landfill and monitoring is mandatory for avoiding exposure to living beings (Nickens et al., 2010). Since the risk of exposure from Cr^{6+}-ions has not been possible to eliminate, the reduction route to extraction of Cr_2O_3 from chromite offers an energy-efficient alternative, as described elsewhere (Escudero-Castejón et al., 2021). The reduction route of chromite in the absence of alkali using carbon for chromium metal production has been also investigated (Cheng et al., 2022; Tian et al., 2022). However, the direct reduction to metal from oxide ores demands much higher temperatures (>1600 °C) and reducing the formation of carbides and silicide of chromium during the chromium-metal and ferrochrome manufacturing (Benz et al., 1974; Kundrat et al., 1984).

The mineralogy of chromite ores is based on the natural spinel structure, composed of 6 spinel compositions ($FeAl_2O_4$, $MgAl_2O_4$, $FeCr_2O_4$, $MgCr_2O_4$, Fe_3O_4 and $MgFe_2O_4$) in solid-solution form (Burns and Burns, 1975). As a result, a range of combinations of solid solution forms of chromite compositions may occur in ore bodies. During alkali reduction, the iron oxide present in the spinel phase is selectively reduced to metallic form (Fe), whereas the Cr_2O_3 in the ore reacts with Na_2CO_3 to form sodium chromite ($NaCrO_2$) in a reducing atmosphere, as shown in reaction (r1).

(r1). $FeCr_2O_{4(s)} + Na_2CO_{3(s)} + 2C_{(s)} \rightarrow Fe_{(s)} + 2NaCrO_{2(s)} + 3CO_{(g)}$.

The main aim of the alkali reduction is to form an iron-rich metallic fraction and a non-metallic fraction containing sodium chromite, sodium aluminate and alkali silicates; which could be subsequently separated by magnetically (Escudero-Castejón et al., 2021). For an efficient magnetic separation, it is necessary to optimize the formation of metallic iron by adjusting the operating parameters of the reduction process.

In the present investigation, the physical chemistry of overall chemical reaction has been analysed in view of the phases formed during the reductive alkali roasting of S. African chromite ore. The rate

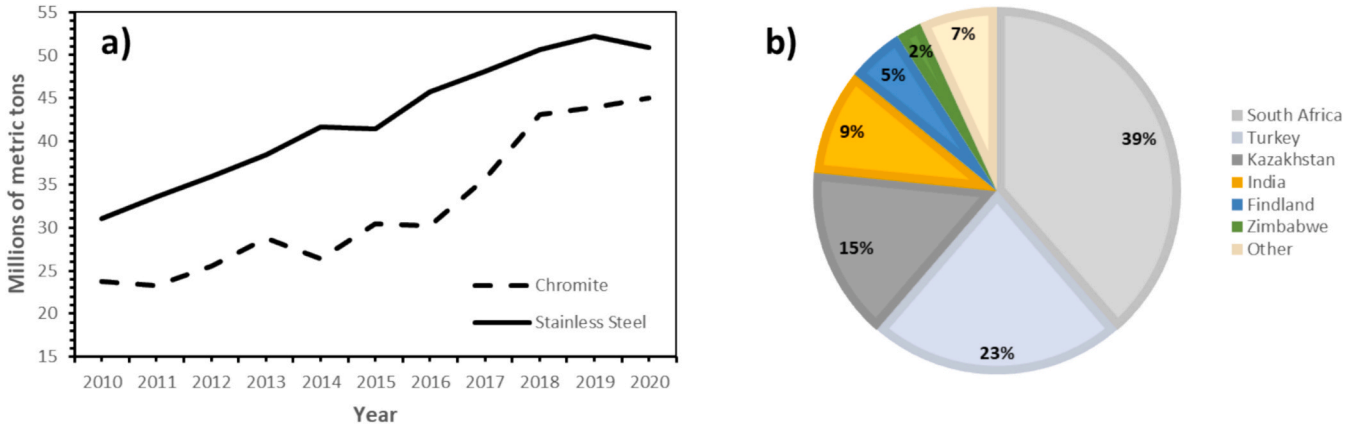

Fig. 1. A) the data on world total output of chromite ores and stainless steel from 210 to 2020 (Statista, n.d.) and b) the main producers of chromite ore in the world (Fastmarkets, n.d).

determining kinetic analysis has been presented for modelling the reactors in future studies.

2. Materials and Methods

2.1. Materials

In this investigation, the composition analysis of the S. African chromite ore is shown Table 1, and the method of analysis has been explained elsewhere (Escudero-Castejón et al., 2021).

Analytical grades of sodium carbonate (99.9 % pure Na_2CO_3) and activated charcoal (carbon content of 99.9 %) were used in the reduction experiments, describe below.

2.2. Experimental methods for the assessment of phase decomposition in s African chromite ores

The phase decomposition studies were carried out by thoroughly mixing in a mortar and pestle the as-received chromite ore with Na_2CO_3 and activated charcoal in a predetermined weight ratios. The powder samples were placed in an alumina crucible and were isothermally reduced in a Carbolite BLF16/3 (UK) tube furnace with a programmable temperature-controlling device for pre-setting both the times and temperatures. The reaction chamber was continuously purged with 2 L/min of argon gas at 2 bars to maintain an oxygen-free atmosphere and prevent oxidation of the samples during the process. After the experiments, the samples were allowed to cool down to room temperature in an oxygen-free atmosphere. The reacted mixture was ground for 30 min to break the agglomerated products. Each ground reacted mixture was analysed phases present using X-ray powder diffraction (PXRD) and Scanning Electron Microscopy.

2.3. Decomposition kinetics of S. African chromite

The isothermal thermogravimetric analysis (TGA) of reaction r1 was carried out in duplicate at different temperatures to analyse the rates of reaction for the kinetic study. For TGA experiments, a 2 g pellet of the reaction mixture was weighed and transferred into an alumina crucible following the procedure described in Escudero-Castejón et al., 2021 (Escudero-Castejón et al., 2021).

2.4. Physical and chemical Characterization of samples

For phase identification before and after reduction reaction in the presence of alkali and carbon, the X-ray powder diffraction (PXRD) technique was adopted. Ground samples were placed in the appropriate sample holder for PXRD analysis using the Philips (USA) X'Pert X-ray diffractometer (Cu-Kα radiation $\lambda = 0.15417$ nm, a step size of $2\theta = 0.03^\circ$ over an angle 2θ between 5° to 85°). The X'Pert HighScore Plus database software supplemented by Reitveld analysis was used for phase identification of the PXRD patterns.

The Carl Zeiss Evo MA 15 Oxford Instruments (UK) Scanning Electron Microscope (SEM) with Aztec Energy dispersive X-ray analytical (EDX) capability was used for the examination of reduced and unreduced chromite ore samples. For SEM analysis, the accelerating voltage was 20 kV with 80 mm X-Max SDD detector for microstructure and semi-quantitative EDX analysis of each sample. For cross-sectional examination of the reaction interface, the powdered sample was dispersed at the bottom of resin-mount cup. The thermosetting Epofix resin and hardener (6:1) was mixed and then gently poured over the powder sample, already placed inside the mould. Once the resin had hardened, the mounted samples were removed from the mould and grinded using silicon carbide papers of different grades (P240-P4000) and finally polished using a Buehler (USA) MetaSeru® 250 machine using different grades of polishing media, to remove cracks. The outer part of the resin-mounted sample was painted with a graphite suspension and then coated with a 5 nm platinum layer to avoid charging during SEM examination.

Table 1
Chemical composition of the as received S. African chromite ore.

Oxide	Weight percentage (%w/w)	Cr:Fe ratio	Particle size (μm)
Cr_2O_3	44.7 ± 2.70	1.7:1	90–120
Fe_2O_3	6.05 ± 1.00		
FeO	18.5 ± 1.82		
MgO	10.9 ± 1.90		
SiO_2	3.8 ± 0.20		
Al_2O_3	14.4 ± 1.90		
TiO_2	0.5 ± 0.01		
V_2O_5	0.3 ± 0.01		
MnO	0.3 ± 0.01		
CaO	0.4 ± 0.01		

3. Results

3.1. Characterization of S. African chromite ore

The PXRD pattern of the as-received chromite ore is shown in Fig. 2, the results shows that the predominant phase is a chromite spinel with Fe^{2+} and Mg^{2+} cations occupying the tetrahedral positions and the Cr^{3+} and Al^{3+} cations in octahedral sites. The reference pattern (01–070-6386) compares well the data in Fig. 2, confirming that the stoichiometric formula of chromite ore is $(Fe_{0.52}Mg_{0.48})(Cr_{0.76}Al_{0.24})_2O_4$ with a lattice parameter of 8.306 Å.

The backscattered SEM images of the as-received chromite ore are presented in Fig. 3. The two phases can be clearly differentiated in these images: light grey particles (A) are chromite spinel particles, and darker grey particles (B) correspond to siliceous gangue minerals. The EDX-SEM elemental analysis of areas A-B is shown in Table 2, which suggests that the composition of chromite ore is consistent with the PXRD of Fig. 1. The gangue phase (number 3 in Fig. 2) is a silicate combined mainly with oxides of aluminium, calcium, and a smaller proportion of sodium, which agrees with elemental mapping results in Fig. 3.

3.2. Phase decomposition studies

3.2.1. Effect of Na_2CO_3 ratio

The stoichiometries of chemical reactions (r1) to (r6) determine the Na_2CO_3:C ratios needed for complexing oxides with alkali and reducing iron oxide to metallic iron. We also investigated the phases formed in different chromite:Na_2CO_3 ratios ranging from 1:0.46 to 1:1 by keeping the chromite:charcoal ratio constant at 1:0.2. For each predetermined chromite, alkali, and charcoal mixture, the temperature and time, were fixed at 1050 °C and 2.5 h respectively.

(r2). $MgCr_2O_{4(s)} + Na_2CO_{3(s)} + C_{(s)} \rightarrow MgO_{(s)} + 2NaCrO_{2(s)} + 2CO_{(g)}$.
(r3). $FeAl_2O_{4(s)} + Na_2CO_{3(s)} + 2C_{(s)} \rightarrow Fe_{(s)} + 2NaAlO_{2(s)} + 3CO_{(g)}$.
(r4). $MgAl_2O_{4(s)} + Na_2CO_{3(s)} + C_{(s)} \rightarrow MgO_{(s)} + 2NaAlO_{2(s)} + 2CO_{(g)}$.
(r5). $MgFe_2O_{4(s)} + Na_2CO_{3(s)} + C_{(s)} \rightarrow MgO_{(s)} + 2NaFeO_{2(s)} + 2CO_{(g)}$.
(r6). $SiO_{2(s)} + Na_2CO_{3(s)} + C_{(s)} \rightarrow Na_2SiO_{3(s)} + 2CO_{(g)}$.

Considering that chromite mineral is a solid solution, the individual spinel members have been considered in reactions r1 to r5 for plotting the Gibbs energy changes against temperature using HSC 5.1 software (Roine, 2002) which results are shown in Fig. 4. Reaction (r6) has also been included to account for the different silica compounds present in the ore.

In Fig. 4, we show that the values of Gibbs energy for reactions (r1) to (r5) are negative above 800 °C. Comparing chromite spinels reactions r1 and r2 above 900 °C, reduction of $FeCr_2O_4$ to form metallic iron and $NaCrO_2$ is more thermodynamically favorable than the reduction of $MgCr_2O_4$. However, the differences are not very significant in the temperature range of 950 °C to 1100 °C. The same tendency is observed in the case of reduction of aluminium-based spinel members, $FeAl_2O_4$ and

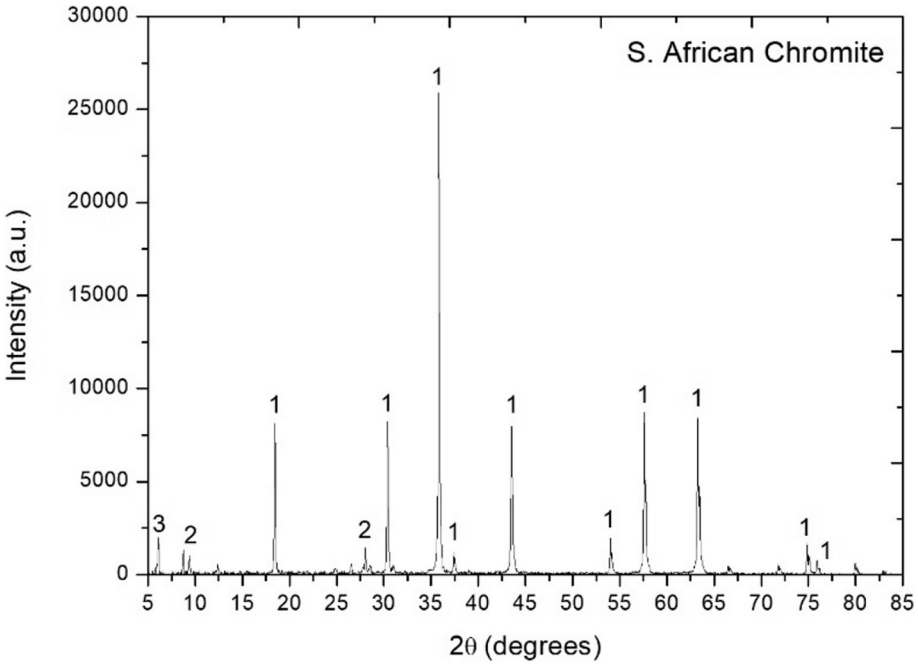

Fig. 2. A PXRD pattern of the as-received chromite ore. 1 = $(Fe_{0.52}Mg_{0.48})(Cr_{0.76}Al_{0.24})_2O_4$, 2 = SiO_2, 3 = $Ca_{11.5}Al_{23}Si_{25}O_{96}$. CuKα radiation.

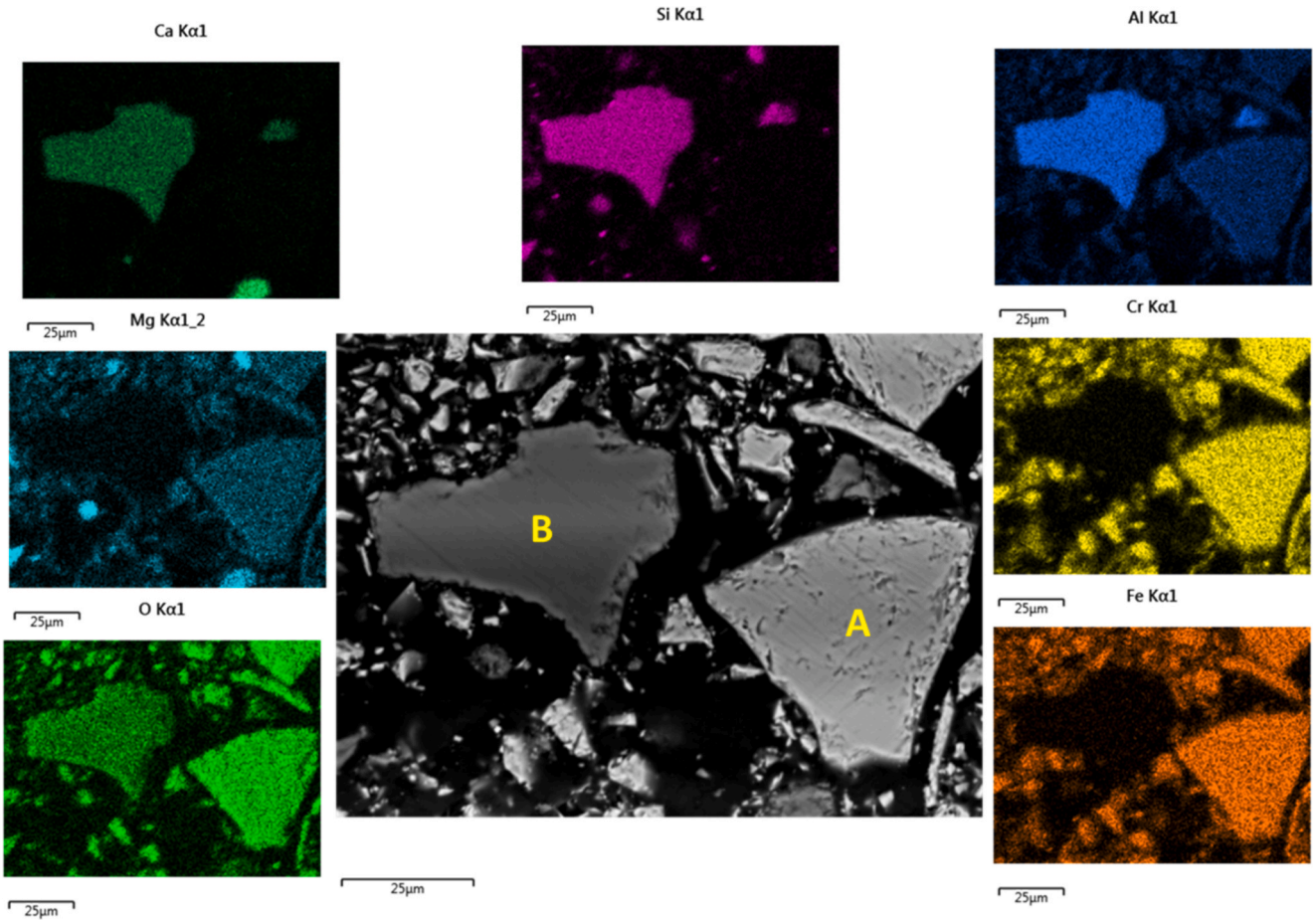

Fig. 3. Backscattered scanning electron microscopy image of the as received chromite ore and elemental distribution map obtained by (EDX).

Table 2
Elemental composition of regions A-B in Fig. 3 analysed by SEM-EDX.

%w/w*	Cr	Fe	O	Al	Mg	Ti	Si	Ca	Na
A	35.2	24.7	24.3	9.5	5.6	0.6	0.0	0.0	0.0
B	0.6	0.3	40.3	17.8	5.8	0.0	26.0	12.4	2.6

*reported standard deviations were ± @.b for Cr, Fe and O and ± @.a for the rest of the elements.

$MgAl_2O_4$ in reactions r3 and r4, in the presence of alkali and carbon. By comparison, the Gibbs energy values for chromium-based spinels are marginally lower than that for the ΔG values of aluminium-based spinels in the entire range of temperatures. From the comparative analysis of the Gibbs energies of decomposition of chromite spinels, it can be deduced that the formation of $NaCrO_2$ is thermodynamically feasible and the difference in the thermodynamic stabilities of $NaAlO_2$ and $NaCrO_2$ appears to be similar for achieving phase separation from the spinel solid solution. The comparative Gibbs energy analysis also demonstrates that $NaFeO_2$, however, is less stable than the alkali complexes $NaCrO_2$ and $NaAlO_2$ in a reducing atmosphere.

The comparative analysis of formation of both $NaCrO_2$ and $NaAlO_2$ is desirable for the alkali reduction process, since $NaCrO_2$ is insoluble in water and it can be separated from metallic Fe by magnetic separation. On the other hand, $NaAlO_2$ is water soluble offering a novel route for soluble-insoluble separation in process flowsheet. The reductive atmosphere during reaction significantly reduces the formation of $NaFeO_2$ which is undesirable as it may co-precipitate both during selective separation of alumina and chromium oxide.

The phases present in the reduced samples were characterised using the powder diffraction method, and these are compared in Fig. 5 and Fig. S1 of the supplementary information. In the mixture compositions with weight ratios equal to 1:0.46 and 1:0.50, both the sodium chromite and metallic iron phases formed. However, in this figure we also confirm the dominance of $MgCr_2O_4$/$MgFe_2O_4$ spinels than that in compositions with higher proportions of charcoal and alkali. The apparent difference in the phase abundance of sodium chromite and metallic iron arises due to the lack of the availability of alkali in the mixture which may not have been able to react with silicates and form sodium silicate via reaction r6. For higher charcoal:alkali ratios, the chromite spinel phases are not present. This is exemplified in the composition ratio chromite:Na_2CO_3 = 1:1 where the main phases present are Fe, $NaCrO_2$, $NaAlO_2$ and MgO. In summary, the results indicate that the excess of Na_2CO_3 is necessary for promoting the formation of sodium chromite and water soluble aluminate, which may help downstream in the physical separation and further purification of phases (Escudero-Castejón et al., 2021).

The SEM images of samples reduced with chromite:Na_2CO_3 weight ratios of 1:0.46, 1:0.67 and 1:1 are compared in Fig. 6 in which the light grey areas represent the iron-rich metallic phases. The areas a-e were analysed by SEM-EDX to compare the chemical composition of the iron-rich metallic phase formed in samples reduced at different weight ratios.

Results presented in Table 3 show the dependence of the solubility limits of metallic Cr as a solute in the iron alloy matrix on the chromite-to-alkali ratio during the reduction process. There is clear evidence from the isothermal reduction reaction data that with increasing alkali in the chromite, the majority of chromium oxide forms sodium chromite, rather than the alloy with more than 12 wt% chromium (Paktunc et al., 2024). This means that an excess of Na_2CO_3 is necessary for increasing the disproportionation of chromium oxide as sodium chromite. On the other hand, for enriching the alloy phase with chromium, more charcoal with chromite:alkali ratio 1:0.5 may be necessary. In the present investigation, based on the mixture compositions investigated, the lowest chromium content in the alloy was below 5 % as reported in areas c to e in Table 3.

3.2.2. *Effect of temperature*

The effect of temperature has been studied in the range of 800 °C to 1100 °C, the weight ratio chromite:Na_2CO_3:charcoal was fixed to 1:1:0.2 and the reduction time was set up to 2.5 h. The powder diffraction phase analysis data are compared in Fig. 7.

At 800 °C, unreacted chromite and sodium carbonate are the main phases present. Part of the iron oxide present in the ore was reduced at this temperature, but most of it has remained in the chromite spinel phase. Although the intensity of diffraction peaks of metallic Fe and $NaCrO_2$ increase with increasing temperatures from 900 °C and above, nevertheless, at 900 °C the unreacted chromite and sodium carbonate were still present. Fig. 8 presents the microscopic evidence for the chemical dissemination of elements during chromite ore decomposition, which then leads to formation of metallic iron and sodium chromite at the phase boundaries of residual iron-depleted spinel phases. Fig. 8a shows the microstructure of chromite particles after being reduced at 800 °C and 900 ^{0}C, respectively. In Fig. 8b, the elemental mapping was obtained by SEM-EDX which indicates that the bright phase is metallic iron while the darker grey phase corresponds to partially reacted chromite phase, which points out that no metallic iron is present at 800 °C, whereas from 900 °C, the formation of metallic iron or alloy commences.

At higher temperatures, the residual chromium-rich phases could not be identified in the powder diffraction patterns in Fig. 7 whereas;the metallic Fe, $NaCrO_2$, $NaAlO_2$, MgO and complex silicates phases were

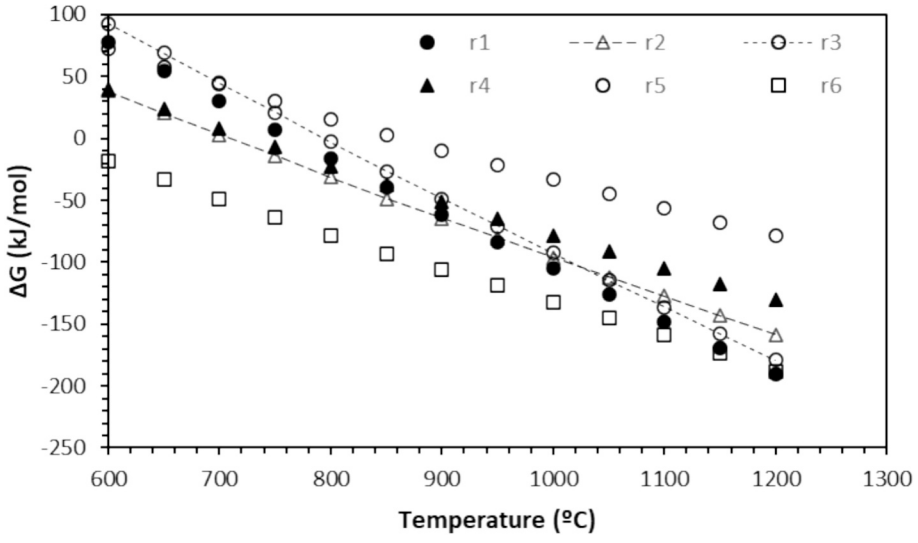

Fig. 4. ΔG versus temperature plot of reactions (r1) to (r6).

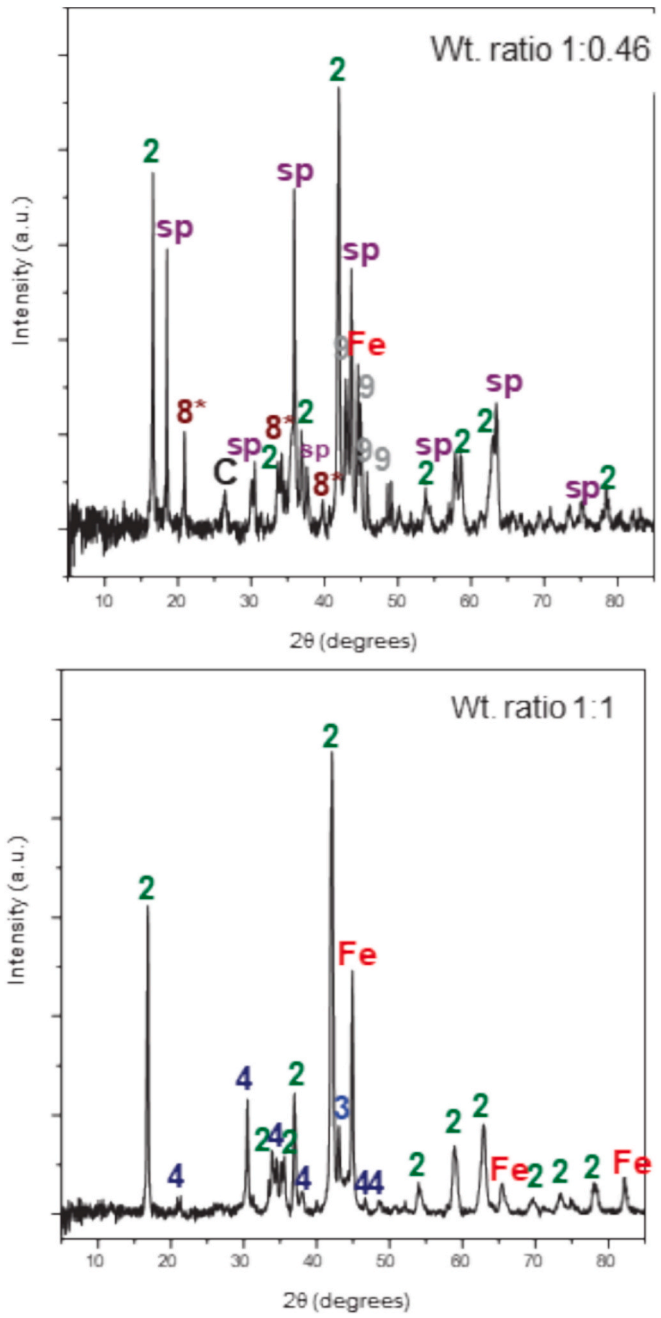

Fig. 5. PXRD patterns of chromite samples after reduction at 1050 °C for 2.5 h using a fixed chromite:charcoal weight ratio of 1:0.2 and a chromite:Na_2CO_3 weight ratios of 1:0.46 and 1:1. [sp = $MgCr_2O_4/MgFe_2O_4$, 2=$NaCrO_2$, 3 = MgO, 4=$NaAlO_2$, 4*=$Na_{1.95}Al_{1.95}Si_{0.05}O_4$, 8*= $Na_2Mg_2Si_2O_7$, 8**= $Na_2Mg_2Si_2O_7$, 9 = Fe_3C, Fe = metallic iron, C = carbon].

found to be more dominant with increasing reduction temperatures.

At 1050 °C, most of the iron oxide was found to have reduced to metallic form by forming larger Fe particles (bright phase) which is exemplified in Fig. 9. Combining the phase analysis shown in Figs. 7 and 8 and the elemental map analysis in Fig. 9, we may be able to conclude that dark grey particles are composed of Cr^{3+} and Al^{+3} ions wherein the Na^+ ions diffuse inwards by forming $NaCrO_2$ and $NaAlO_2$. Part of the magnesium oxide diffuses out to form a MgO-rich rim and the rest of it combines with silica to form complex silicates.

3.2.3. Effect of time

The progress of the chromite reduction reaction was also studied with increasing time period by carrying out investigations under a chosen isothermal condition, for example, at 1050 °C for a fixed weight ratio of chromite:Na_2CO_3:charcoal = 1:1:0.2. As observed in Fig. 10, the PXRD peaks for metallic iron can be observed after 15 min of reaction, which indicates that reduction of iron oxide in chromite to metallic form occurs rapidly at a temperature of 1050 °C, which was also evident from the SEM analysis of the partially reduced sample. As the reduction reaction proceeds, more metallic iron forms as fine needles inside chromite particles which may be observed in Fig. 11. The micro-crystallites of metallic iron start clustering and these crystallites then continue to grow with time. Eventually, they may separate from the reduced chromite and form round metallic particles, which is the preferred form for subsequent magnetic separation. The metallic iron predominantly formed during reduction is ferrite (α-Fe), however, formation of austenite (γ-Fe) can be observed at 1 and 1.5 h due to a fast cooling which leads to a metastable γ-Fe phase. The difference in the diffraction peaks of α-Fe and γ-Fe is feasible by using the PXRD technique, since both phases are allotropes of metallic iron with different crystal structure. The γ-Fe is the allotrope formed between 950 °C and 1050 °C. On cooling the samples, to ambient temperature, it was observed that the γ-Fe should transform to α-Fe during the cooling process(Boi et al., 2017). The α-Fe is the predominant and desirable form since it has the best magnetic properties; and therefore, any γ-Fe should be avoided to improve the efficiency of the magnetic separation.

We observed that not all metallic iron may be possible to separate even after 6 h reaction. This type of microstructure is a manifestation of diffusion barrier which is increasing with increasing inter-particulate distance and resembles with the theory of Ostwald ripening (Voorhees, 1985). Formation of $NaCrO_2$ can be also seen after 15 min of reaction. After 30 min, unreacted chromite cannot be identified in the PXRD pattern in Fig. 10. When reduction is carried out during 2.5, 3.5 or 6 h, the main phases present are $NaCrO_2$, Fe, MgO and $NaAlO_2$. Based on this, 2.5 h has been chosen as the optimum roasting time.

3.2.4. Effect of activated charcoal ratio

The effect of activated charcoal on the reduction of chromite in the presence of sodium carbonate was also studied by carrying out the reduction experiments with different chromite:charcoal weight ratios. The weight ratio of chromite:Na_2CO_3 was constant for all the experiments and equal to 1:1, temperature was fixed at 1050 °C and each sample was reduced for 2.5 h. The PXRD patterns of the reduced samples are compared in Fig. 12.

The reduction of iron is not complete when a chromite:charcoal weight ratio of 1:0.08 is used. However, when it was increased up to 1:0.33, a better reduction of iron oxides was achieved. Above 1:0.33, the formation of metallic iron starts decreasing again. This might be due to the increased amount carbon in the mixture with deficient sodium carbonate in the mixture. The observation again reinforces that it is the optimised concentrations of chromite to alkali which must be balanced against overall carbon for producing CO gas when the sodium carbonate starts decomposing above 800 °C (Tian et al., 2025). The formation of $NaCrO_2$ is observed for all different ratios, and the formation of sodium and magnesium silicates and (Ca,Mg)CO_3 increases when the ratio of carbon is high (1:0.33 and above). According to the results obtained, the chromite:charcoal weight ratio should be in the range of 1:0.17 to 1:0.25.

3.3. Kinetics of the alkali reduction of S. African chromite

3.3.1. Isothermal thermogravimetric analysis

The degree of reduction (X) was calculated based on the isothermal thermogravimetric experimental data collected at different temperatures. Experiments at temperatures of 800 °C, 850 °C, 900 °C, 950 °C, 1000 °C and 1050 °C were carried out with a chromite:Na_2CO_3:charcoal weight ratio of 1:1:0.2. The weight loss was recorded with time during each experiment (observed weight loss), and this data was used to

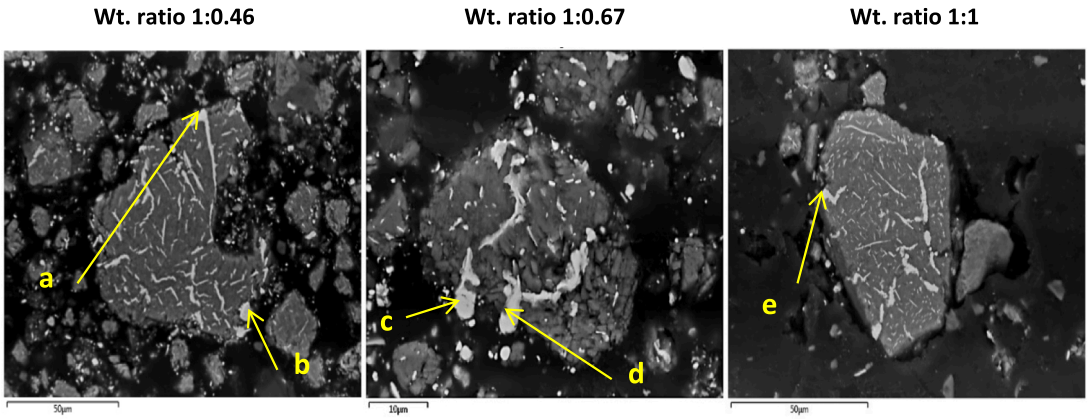

Fig. 6. Backscattered SEM images of reduced chromite samples at 1050 °C for 2.5 h with three different chromite:Na_2CO_3 weight ratios (1:0.46, 1:0.67 and 1:1). Chromite:charcoal wt. ratio = 1:0.2.

Table 3
Chemical composition of areas a-e in Fig. 5 analysed by SEM-EDX.

Area	a	b	c	d	e
Chromite:Na_2CO_3 wt. ratio	1:0.46		1:0.67		1:1
wt.% Fe	87.2	84.6	95.9	95.7	95.2
wt.% Cr	12.8	15.4	4.1	4.3	4.8

*reported standard deviations were ± 0.2 for Cr and Fe.

calculate X following equation (eq.1).

$$X(\%) = 100^{*}\left(\frac{Observed\ weight\ loss(g)}{Theoretical\ weight\ loss(g)}\right) \quad (1)$$

The theoretical weight loss was calculated using the stoichiometric calculations based on the composition of the chromite ore, the alkali and carbon weight ratios in the reaction mixture, the initial weight of the sample and the weight loss expected from reactions (r7) to (r11)

(r7). $FeO_{(s)} + C_{(s)} \rightarrow Fe_{(s)} + CO_{(g)}$.

(r8). $Fe_2O_{3(s)} + 3C_{(s)} \rightarrow 2Fe_{(s)} + 3CO_{(g)}$.

(r9). $Cr_2O_{3(s)} + Na_2CO_{3(s)} + C_{(s)} \rightarrow 2NaCrO_{2(s)} + 2CO_{(g)}$.

(r10). $Al_2O_{3(s)} + Na_2CO_{3(s)} + C_{(s)} \rightarrow 2NaAlO_{2(s)} + 2CO_{(g)}$.

(r11). $Na_2CO_{3(s)} + C_{(s)} \rightarrow Na_2O_{(s)} + 2CO_{(g)}$.

If excess sodium carbonate is present in the reaction mixture, the weight loss due to the decomposition of Na_2CO_3 following reaction (r11) needs to be considered. A detailed study of the thermal decomposition of sodium carbonate was conducted by Motzfeldt (Motzfeldt, 1955). The isothermal thermogravimetric plots in Fig. 13 for the S. African chromite are shown for temperatures of 800 °C and 850 °C. From this figure, the degree of reduction increases steadily with time (t, hour). Above 900 °C, the fraction reacted increases rapidly before it reaches a plateau where the reaction halts. At the higher temperatures, for example 1050 °C, the reaction occurred rapidly and achieved a maximum degree of reduction

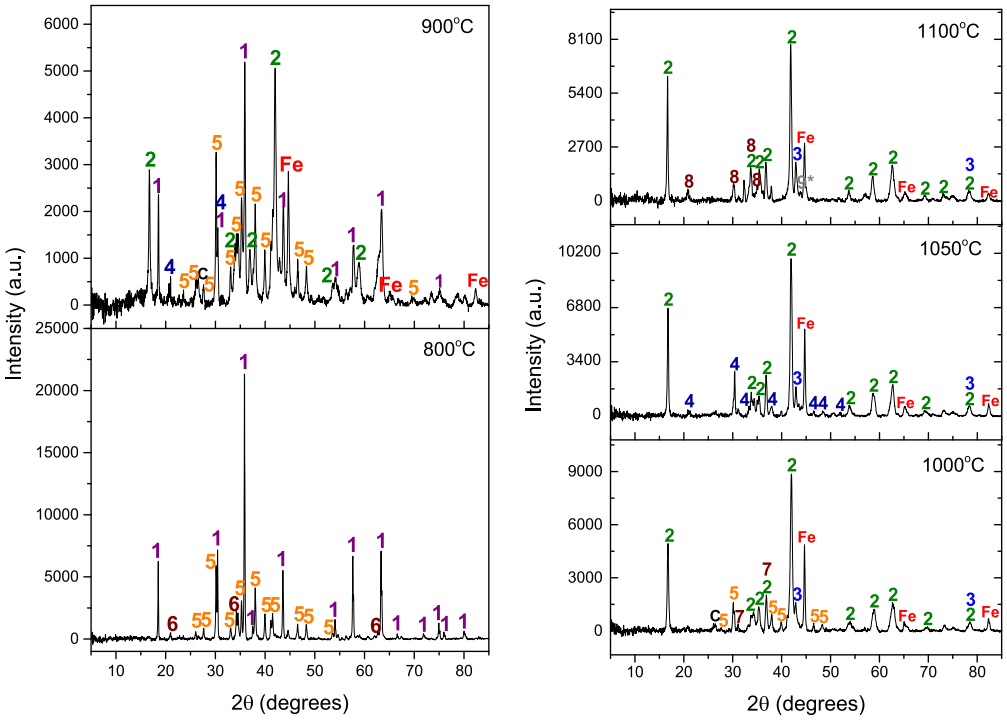

Fig. 7. The PXRD patterns of samples after reduction at 800 °C, 900 °C, 1000 °C, 1050 °C and 1100 °C are compared for a Chromite:Na_2CO_3:charcoal weight ratio of 1:1:0.3. The phases identified are [1=$(Fe_{0.5}Mg_{0.5})(Cr_{0.73}Al_{0.27})_2O_4$, 2=$NaCrO_2$, 3 = MgO, 4=$NaAlO_2$, 5=$Na_2CO_3$, 6=$Na_{0.87}Mg_{0.4}Al_{0.07}Si_{0.53}O_2$, 7=$(Fe,Mg)_2SiO_4$, 8=$Na_{1.8}Mg_{0.9}Si_{1.1}O_4$, 9*=$FeC_{0.045}$, Fe = metallic iron, C = carbon].

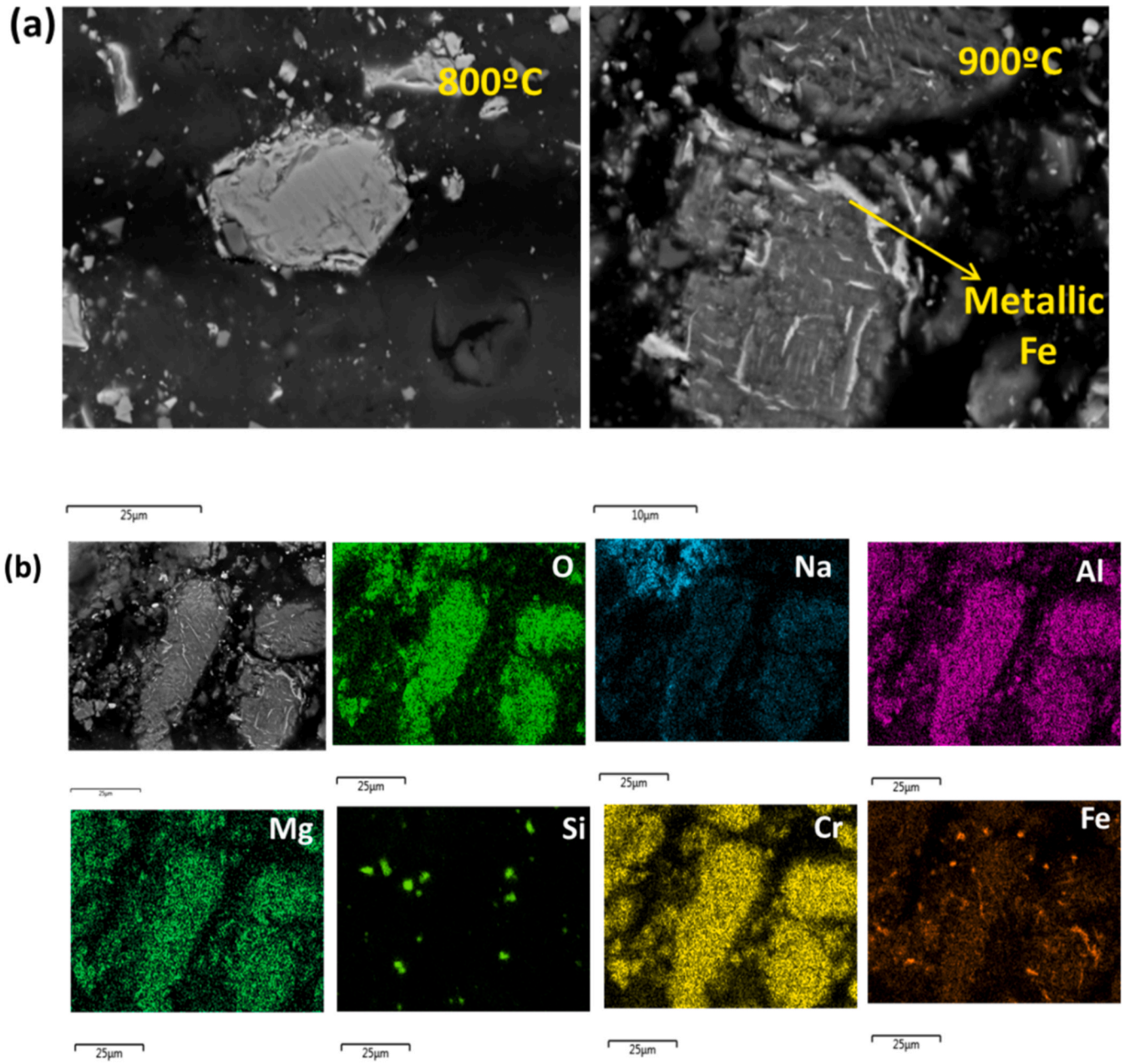

Fig. 8. (a) Backscattered SEM images of chromite after reduction with Na_2CO_3 and activated charcoal at 800 °C/900 °C, and (b) Elemental mapping after reduction with Na_2CO_3 and activated charcoal at 900 °C.

of approximately 92 % after 30 min.

3.3.2. Determination of reaction rate and activation energy

Based on the thermogravimetric experimental data, different kinetic models for diffusion-controlled and reaction-controlled solid-state reactions were analysed and compared. In the case of the diffusion control model, where the rate-limiting step may be the diffusion of ions through the product layer. Ginstling and Brounshtein (GB) (Ginstling and Brounshtein, 1950), proposed the following equation (eq.2):

$$1 - \frac{2}{3} \bullet X - (1 - X)^{\frac{2}{3}} = k_1 \bullet t \quad (2)$$

When the reaction at the particle interface is the rate-limiting step, the equation (eq.3) developed by Spencer and Topley (ST) (Spencer, Wilfred Devonshire; Topley, 1929), may be applied:

$$1 - (1 - X)^{\frac{1}{3}} = k_2 \bullet t \quad (3)$$

A mixed kinetic control including both diffusion and reaction control can be also considered, in which case the kinetic equation would be the following:

$$(1 - \frac{2}{3} \bullet X - (1 - X)^{\frac{2}{3}}) + (1 - (1 - X)^{\frac{1}{3}}) = k_3 \bullet t \quad (4)$$

In equations (eq.2), (eq.3) and (eq.4), X stands for the fraction reacted or degree of reduction, k_i for the respective rate constants (min^{-1}) and t for the reaction time (min). The experimental data from the X versus time (t) curves in Fig. 13 were taken every 5 min and fitted to equations (eq.2), (eq.3) and (eq.4), for the GB, ST and mixed model, respectively. The last section of the curves, where a plateau is reached, was not included in the fitting as the reaction is considered to stop when no

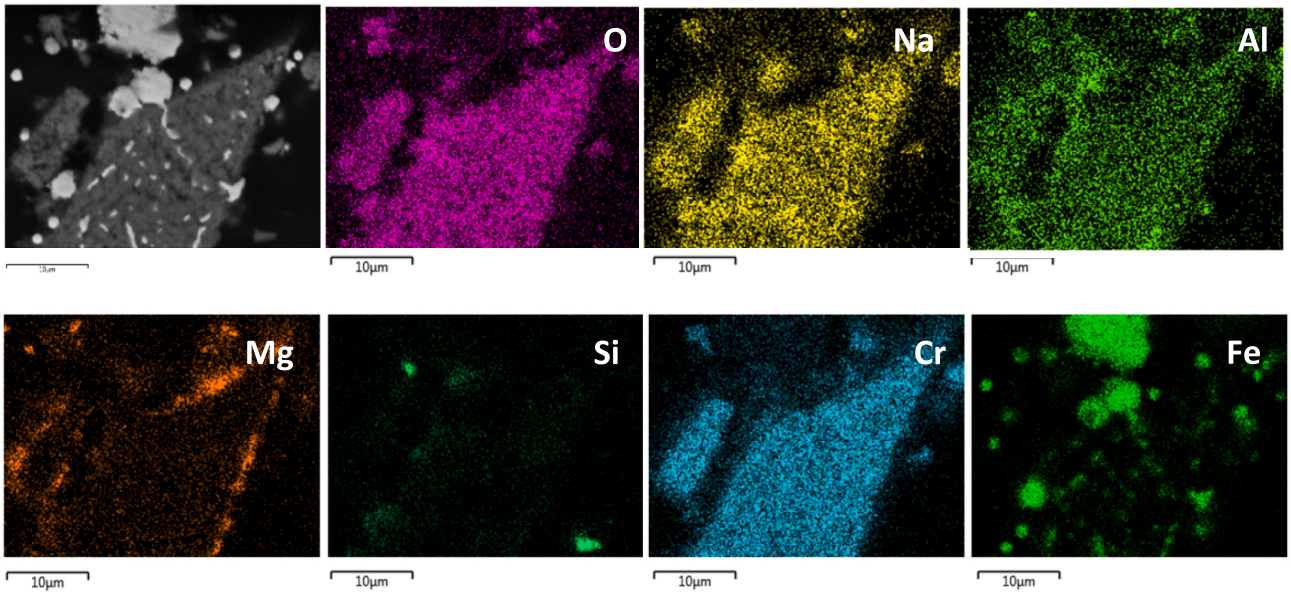

Fig. 9. Elemental mapping of chromite sample reduced with activated charcoal and sodium carbonate at 1050 °C.

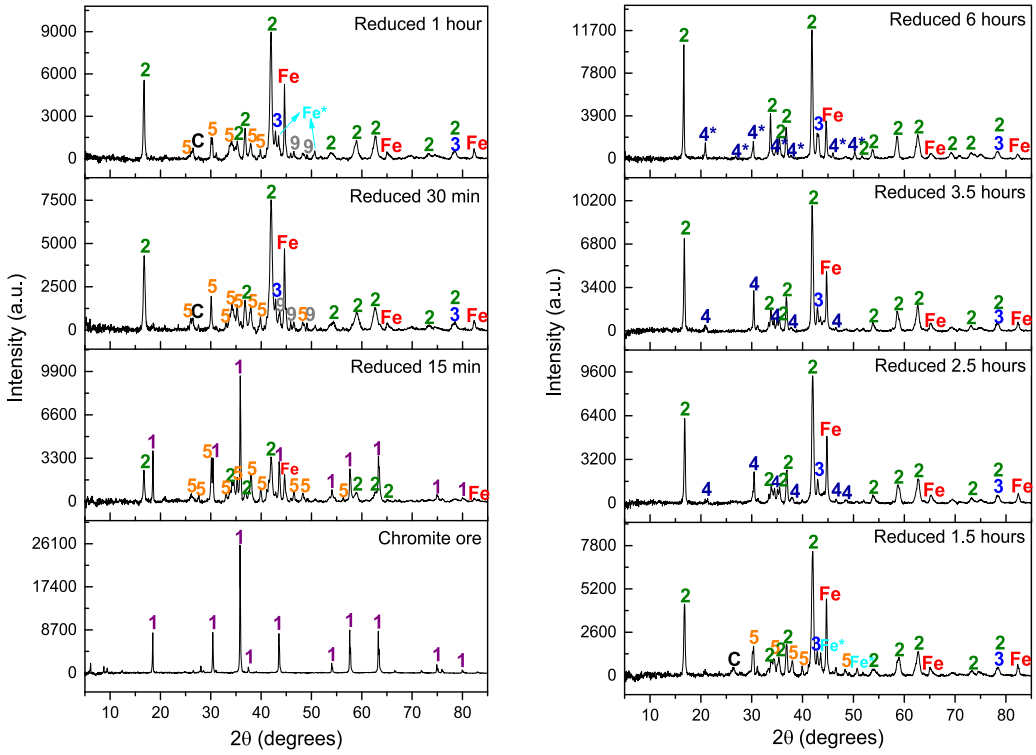

Fig. 10. PXRD patterns of as-received chromite and reduced samples after reduction at 1050 °C with weight ration chromite:Na_2CO_3:charcoal = 1:1:0.2 for different times. [1=$(Fe_{0.5}Mg_{0.5})(Cr_{0.73}Al_{0.27})O_4$, 2=$NaCrO_2$, 3 = MgO, 4=$NaAlO_2$, 4*=$Na_{1.95}Al_{1.95}Si_{0.05}O_4$, 5=$Na_2CO_3$, 9 = Fe_3C, Fe/Fe*=α/γ metallic iron, C = carbon].

weight loss is observed.

Comparing the data in the plots in Fig. 14, it is evident that the Ginstling and Brounshtein model fits to the experimental data much better than the ST and mixed models. The statistical analysis confirms that the R-squared values always are at least 0.99 for all the GB-model fitted data, which confirms that the reduction of S. African chromite with alkali is a diffusion-controlled process. The activation energy (E_a) of the reduction reaction can be calculated by using the Arrhenius equation shown below in (eq.5). The Arrhenius activation energy analysis is based on plotting the natural logarithm of the constant rates obtained from the GB model against the reciprocal of the absolute temperature ($\frac{1}{T}$) (1073 K-1323 K), as shown in Fig. 15.

$$\ln k = \ln A - \frac{E_a}{R} \bullet \frac{1}{T} \quad (5)$$

The activation energy obtained from the slope of the linear relationship in Fig. 15 for the alkali reduction of S. African chromite ore is 206.0 ± 0.8 kJ/mol. The activation energy calculated in this study for the

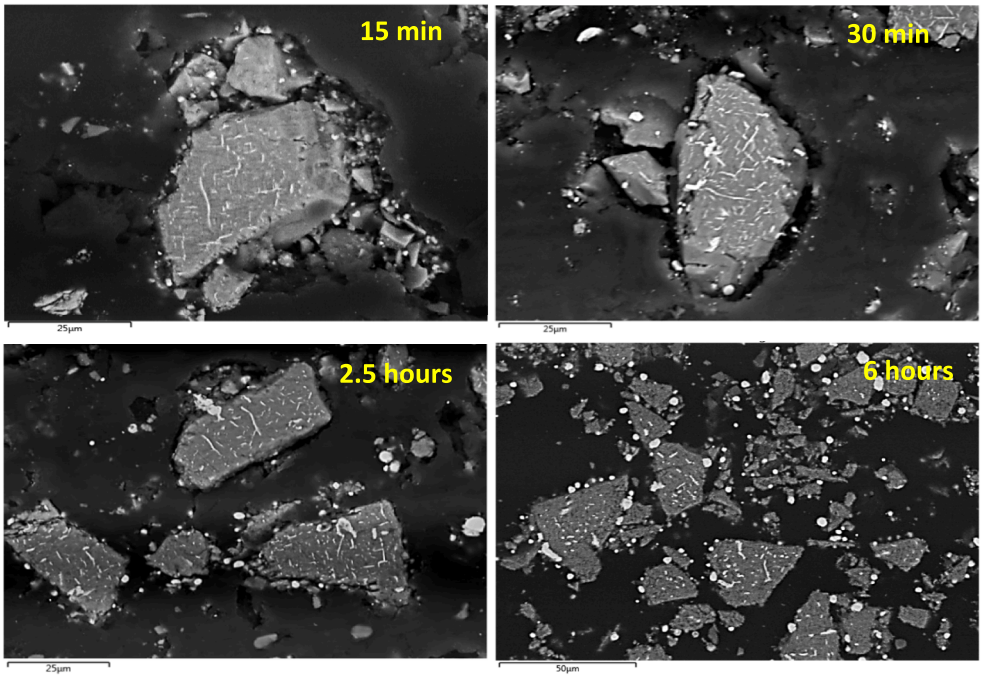

Fig. 11. Backscattered SEM images of chromite after reduction with Na_2CO_3 and activated charcoal at 1050 °C during 15 min, 30 min, 2.5 h and 6 h (weight ratio chromite:Na_2CO_3:charcoal = 1:1:0.2).

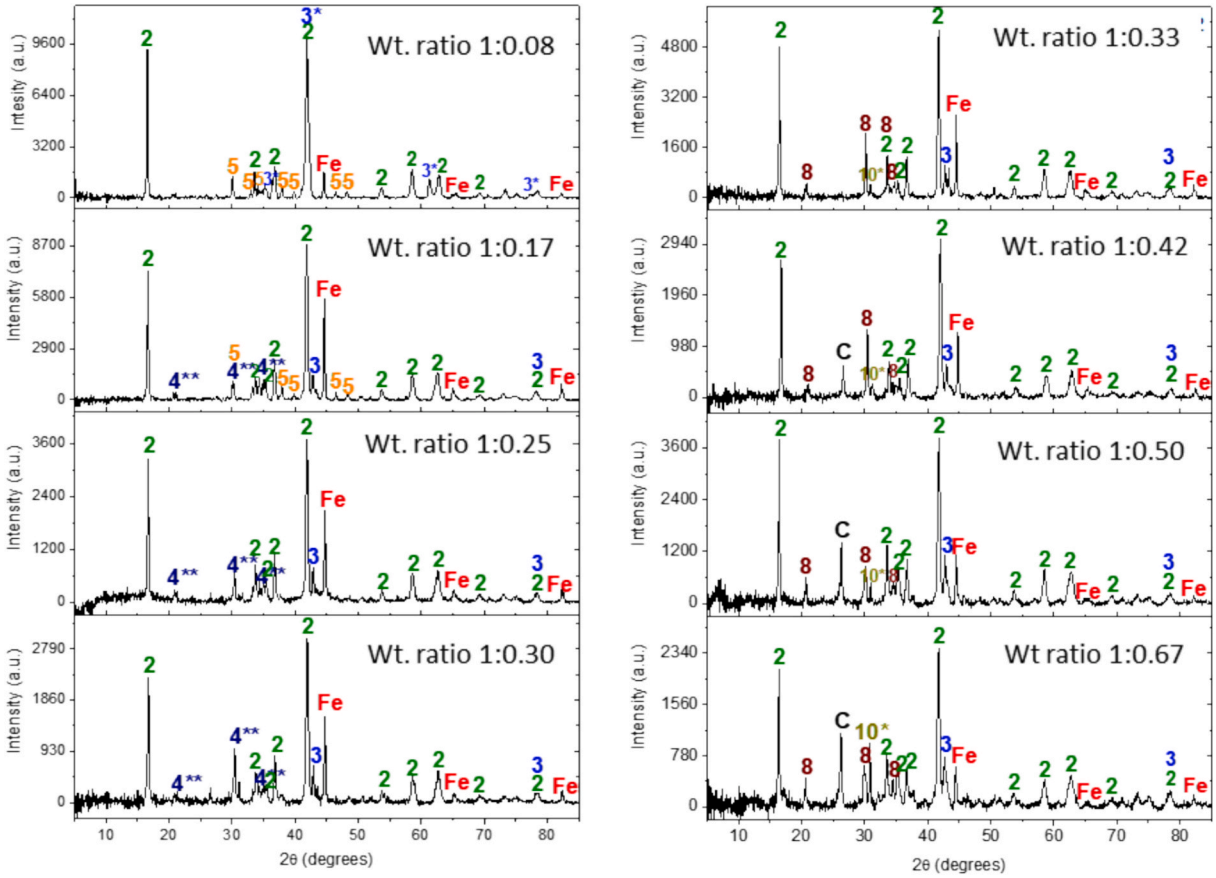

Fig. 12. PXRD patterns of chromite samples after reduction at 1050 °C for 2.5 h using different chromite:charcoal weight ratios. [2=$NaCrO_2$, 3 = MgO, 3*=(Mg,Fe)O, 4**=$Na_{1.5}AlSiO_{4.25}$, 5=Na_2CO_3, 8= $Na_{1.8}Mg_{0.9}Si_{1.1}O_4$, 10*=$(Ca,Mg)CO_3$, Fe = metallic iron, C = carbon].

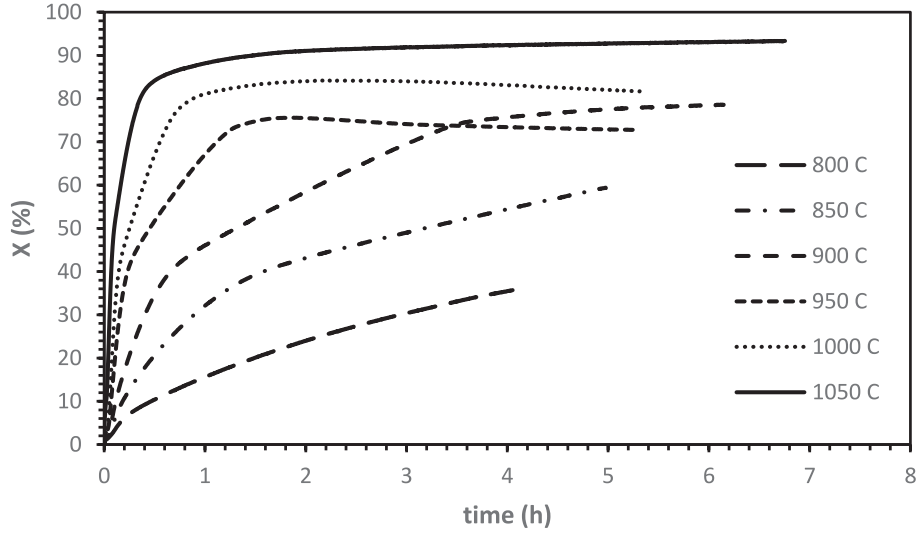

Fig. 13. (%) Reduction vs time curves for the carbothermic reduction of S. African chromite ore in the presence of Na_2CO_3 at constant temperature with a chromite: Na_2CO_3:charcoal weight ratio of 1:1:0.2.

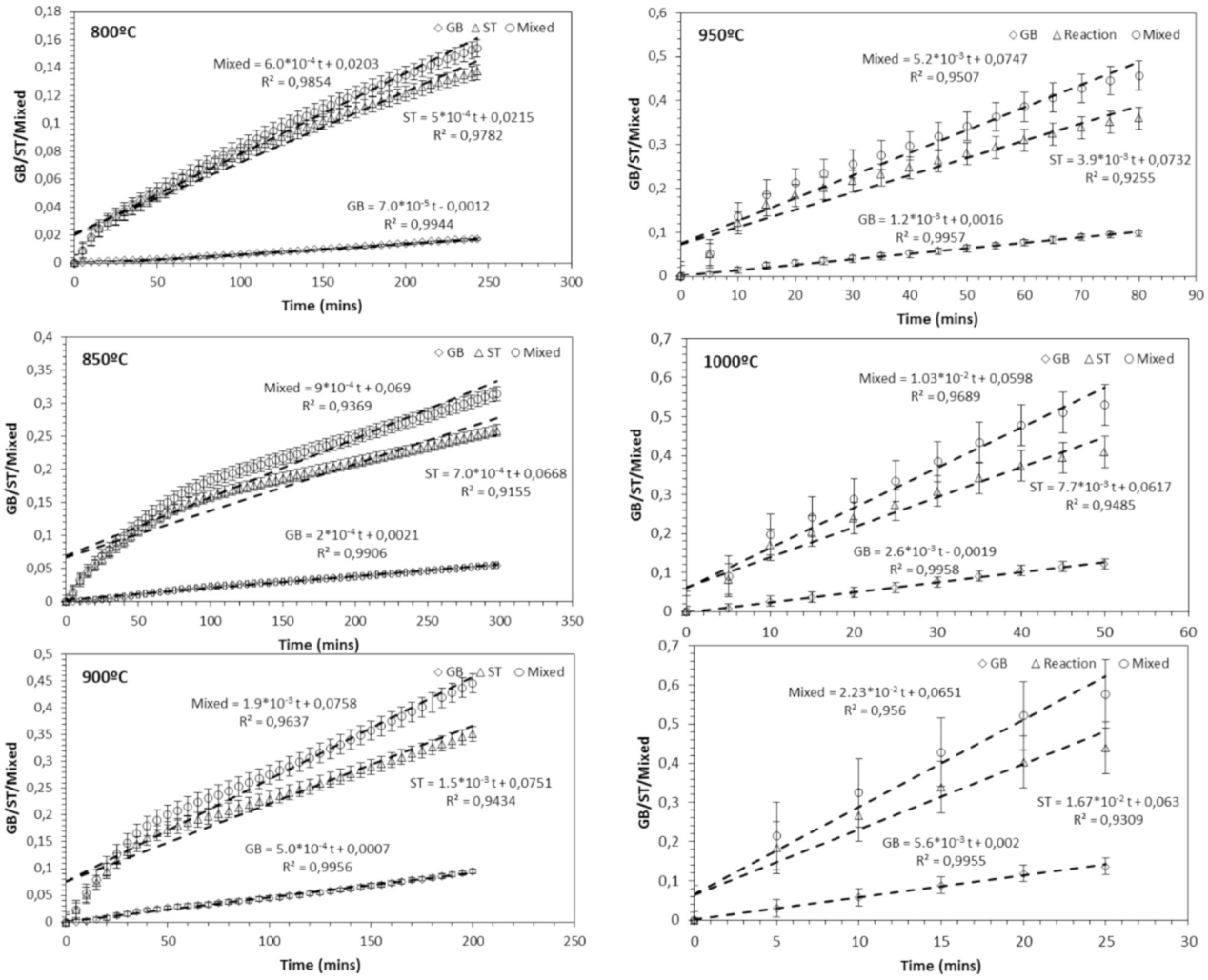

Fig. 14. Ginstling and Brounshtein (GB), Spencer and Topley (ST) and mixed model equations versus time from experimental TGA data collected with S. African chromite.

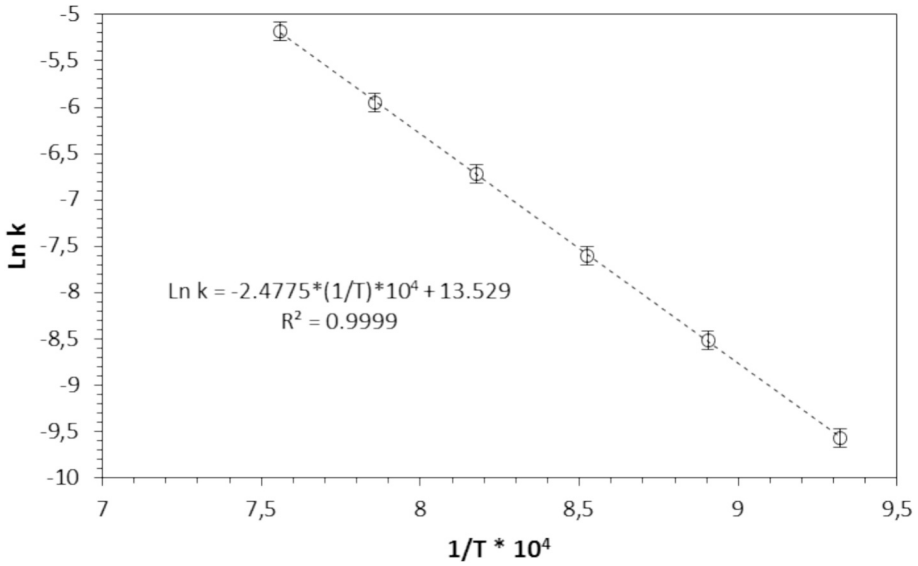

Fig. 15. Arrhenius plot of S. African chromite ore reduction.

reductive roasting of S. African chromite in the presence of Na_2CO_3 is comparable to that obtained by Kekkonen et al. (1995), and Ding and Warner, 1997a (Ding and Warner, 1997a), who studied the reduction kinetics of carbothermal reduction with CO gas of chromite pellets at much higher temperatures (in the range of 1420 °C to 1595 °C), and also used the unreacted core model to explain the mechanism of reduction. This means that the presence of alkali in the reduction reaction enables the possibility of operating at significantly lower temperatures compared to traditional processes of carbothermic reduction of chromite ore. Moreover, the microstructures shown by Kekkonen et al. (1995) are similar to the observed in this study. The E_a values of chromite reduction calculated by previous investigations from different authors are summarised in Table 4.

Tathavadkar et. al 2001 (Tathavadkar et al., 2001) carried out the soda-ash roasting of S. African chromite in oxidizing, inert and reducing atmosphere. They reported the formation of $NaCrO_2$ in all cases with the difference that in air, further oxidation of $NaCrO_2$ to Na_2CrO_4 occurs. For the oxidative process, they estimated an activation energy of 185 ± 5 kJ/mol at temperatures ranging between 750 and 937 °C reaching the conclusion that Cr^{3+} solid state diffusion was the limiting step of the process. In fact, according to Tathavadkar et. al 2001 (Tathavadkar et al., 2001) the activation energy for the solid state diffusion of Cr^{3+} ions in chromite should be between the octahedral crystal field stabilization energy (CFSE) which is 225 kJ/mol and the octahedral site preferential energy (OSPE) which is 158 kJ/mol. For the reductive alkali roasting of S. African chromite conducted in this work an activation energy of 206 kJ/mol was calculated which agrees with Tathavadkar et. al 2001 observations (Tathavadkar et al., 2001).

Table 4
Previous findings on the kinetics of chromite reduction. Table adapted from Wang et al. (2014).

Additive	Controlling mechanism	E_a (kJ/mol)	Reference
None	Early stage: nucleation/ chemical reaction Late stage: gas/solid diffusion	114 221	(Ding and Warner, 1997a)
None	Unreacted core with gas/solid diffusion	224	(Kekkonen et al., 1995)
None	Diffusion of oxygen	57	(Murti and Seshadri, 1982)
CaO	Early stage: nucleation/ chemical reaction Late stage: diffusion of Cr	139–161 410	(Ding and Warner, 1997a)
SiO_2	Early stage: diffusion of ions Late stage: smelting of Cr	194 256	(Ding and Warner, 1997a)
SiO_2	Early stage: nucleation/ chemical reaction Late stage: not found	172	(Duong and Johnston, 2000)
None	Low T: Pore diffusion + interfacial reaction High T: Chemical reaction	420	(Xiao et al., 2001)

3.3.3. *Reaction mechanism of the reductive alkali roasting of S. African chromite*

The mechanism proposed for the reductive alkali reduction of S. African chromite is discussed based on the experimental observations presented in this work and previous literature review. The proposed reaction mechanism consists of the following steps:

1. Boudouard reaction and decomposition of Na_2CO_3.
2. Diffusion of the gaseous reductant (CO) through the gas film around the chromite particle and through the porous solid and cracks towards the reaction surface.
3. Adsorption of the gaseous reductant on the reaction surface.
4. Diffusion of Fe^{2+}/Fe^{3+} and O^{2-} through the vacancies of the structure and towards the reaction surface.
5. Chemical reaction on the reaction surface between the gaseous reductant and the oxygen in the chromite spinel lattice leading to metallisation of Fe.
6. Reaction of sodium oxide with Al^{+3} ions to form $NaAlO_2$.
7. Diffusion of Mg^{2+} ions through the vacancies in the spinel structure towards the outer rim of the chromite particle, and formation of MgO phase.
8. Diffusion of sodium ions via the voids in the spinel structure towards the reaction surface and reaction with Cr^{+3} to form $NaCrO_2$.
9. Desorption of the gaseous reaction product (CO_2 gas) from the reaction surface.
10. Diffusion of the gaseous reaction product through the porous solid or cracks of the chromite particle, and through the gas film around the particle.

During carbothermal reduction of chromite, the carbon gasification by the Boudouard reaction may be controlling the kinetics in the early stages of the process, as the replacement rate of the CO consumed on the reaction front depends on the rate of this reaction. If the Boudouard reaction is limiting the early stages of reduction a higher concentration

of CO_2 is expected in the gas. The catalytic effect of alkali carbonates on the Boudouard reaction has been previously reported in literature (Rao, 1983; von Bogdandy and Engell, 1971), indicating that the presence of sodium carbonate might increase the rate of reduction. The diffusion of gaseous CO through the gas film is expected to be a limiting factor of the reaction rate, especially when a silicate product layer around chromite particles is formed (Antony et al., 2006). The alkali present during reduction is, however, able to promote the breakage and cracking of the chromite particle and therefore the metallisation of $Fe^{2+/3+}$ by CO gas is increased. The formation of metallic Fe spheres at the edges of the partially reduced particles was reported as the rate limiting factor by Niayesh and Dippenaar 1992 (Niayesh, 1992), as it can limit the diffusion of gases through the product-layer. In this case the formation of the metallic phase occurs first as needle-shape metallic Fe within the $NaCrO_2$/$NaAlO_2$ matrix, which later diffuses towards the edge or grows within internal cracks formed because of reduction. Rounded metallic particles are then formed at the border or in the cracks of the reduced particles in the last stages of the reaction. The metallic particles, however, tend to separate once in the surface and do not form a continuous rim. Therefore, this is not expected to be a limiting factor in this case.

The reaction between CO and the oxygen from the lattice leads to the formation of CO_2 yielding $2e^-$, which are responsible for the reduction of Fe^{2+} to metallic Fe^0. The reduction process is expected to create vacancies, increasing the reactivity of chromite. Reaction could be a limiting factor, however, previous publications on the carbothermal reduction of chromite agreed on the fact that reduction of Fe_2O_3 and FeO occurs in first place, followed by the reduction of Cr_2O_3 once metallisation of iron is completed (Dawson and Edwards, 1986; Ranganathan et al., 2011; von Bogdandy and Engell, 1971). In the case of alkali reduction of chromite, the presence of alkali minimises the formation of metallic Cr by forcing the equilibrium towards the formation of $NaCrO_2$ phase, and hence only a small fraction of chromium is metallised forming the Fe-Cr metallic alloy, as shown in section 3.2.1. Limited formation of Cr metal is an advantage of the alkali reduction over carbothermal reduction in the absence of alkali, as metallisation of Cr, which is the slow step, is not desired. It was observed that the diffusion of Na^+ ions from the edges of the particle towards the centre occurs rapidly. Formation of $NaCrO_2$ can be observed after 15–30 min of reaction, as it was indicated by PXRD patterns presented in Fig. 9.

Previous research carried out on the oxidative roasting of chromite ores studied the effect of Fe/Mg replacement on the extraction of chromium as Na_2CrO_4. It was found that the replacement of Fe^{2+} by Mg^{+2} in the spinel structure has no significant effect on the chromium extraction (Thompson and Lawson, 1984). On the other hand, Tathavadkar et al. 2003 (Tathavadkar et al., 2003) found that the higher the fraction of Mg^{2+} in the chromite spinel, the lower is the extraction yield observed. The author concluded that there is a detrimental effect for chromite spinels rich in Mg. The reduction of Mg-based spinels, namely $MgCr_2O_4$ and $MgAl_2O_4$, in the presence of Na_2CO_3 and charcoal is less thermodynamically favourable than that of Fe-base spinels ($FeCr_2O_4$, $FeAl_2O_4$) (Escudero-Castejón et al., 2021). $MgCr_2O_4$ presents high stability at high temperatures under reducing conditions and in the presence of alkali, which may be explained by the need of balancing between divalent and trivalent ions in the spinel lattice.

4. Conclusions

The main conclusions of this study can be summarised as follows:

- The effect of process parameters on the reductive alkaline roasting of S. African chromite ore were studied, obtaining the best results for a chromite:Na_2CO_3:charcoal weight ratio of 1:1:0.2, a temperature of 1050 °C and a reduction time of 2.5 h.
- The kinetic study of the alkali reduction of S. African chromite suggests that the kinetics of the reaction can be described by the GB model with an Ea value of 206.0 ± 0.8 kJ/mol.
- The mechanism of the reduction of chromite in the presence of alkali is similar to the direct carbothermic reduction of chromite. However, this work has demonstrated that the presence of alkali promotes iron reduction inducing cracks in the mineral particles and therefore increasing the reaction specific surface. Chromium reduction is the slowest reaction during the direct carbothermic reduction of chromite, so as, it represents the limiting step of the process. The addition of alkali avoids this step through the formation of $NaCrO_2$ which is a fastest reaction.
- The activation energy determined in the range of 800 to 1050 °C for the carbothermic reduction of chromite in the presence of alkali is similar to the value reported by Tathavadkar et. al 2001 (Tathavadkar et al., 2001) for the oxidative roasting in the range of 750 to 973 °C suggesting that Cr^{3+} ions diffusion is the rate limiting step.

CRediT authorship contribution statement

S. Sanchez-Segado: Writing – original draft, Formal analysis, Supervision, Writing – review & editing, Methodology, Visualization, Data curation. **L. Escudero-Castejón:** Methodology, Writing – original draft, Formal analysis, Validation, Investigation. **A. Jha:** Supervision, Formal analysis, Methodology, Writing – review & editing, Funding acquisition, Resources, Conceptualization.

Declaration of competing interest

The authors declare that they have no known competing financial interests or personal relationships that could have appeared to influence the work reported in this paper.

Acknowledgements

The authors acknowledge the financial support received from the -Leeds Doctoral Training PhD (DTP) Scholarship for LE-C, NERC SoS-RARE (NE/M01147X/1), Catalyst Grant (NE/L002280/1) and the Marie-Curie IIF E4-Crit-Mat project (Grant agreement 331385).

Appendix A. Supplementary data

Supplementary data to this article can be found online at https://doi.org/10.1016/j.mineng.2025.109595.

Data availability

Data will be made available on request.

References

Antony, M.P., Jha, A., Tathavadkar, V., 2006. Alkali roasting of Indian chromite ores: thermodynamic and kinetic considerations. Miner. Process. Extr. Metall. 115, 71–79. https://doi.org/10.1179/174328506X109086.

Antony, M.P., Tathavadkar, V.D., Calvert, C.C., Jha, A., 2001. The soda-ash roasting of chromite ore processing residue for the reclamation of chromium. Metall. Mater. Trans. B 32, 987–995. https://doi.org/10.1007/s11663-001-0087-6.

Azimi, G., Shamanian, M., 2010. Effects of silicon content on the microstructure and corrosion behavior of Fe–Cr–C hardfacing alloys. J. Alloys Compd. 505, 598–603. https://doi.org/10.1016/j.jallcom.2010.06.084.

Benz, R., Elliott, J.F., Chipman, J., 1974. Thermodynamics of the carbides in the system Fe-Cr-C. Metall. Trans. 5, 2235–2240. https://doi.org/10.1007/BF02643938.

Boi, F.S., Hu, Y., Wen, J., 2017. New insights on the dynamics of the γ-Fe/α-Fe phase-transition inside iron-filled carbon nanotubes. RSC Adv. 7, 25025–25030. https://doi.org/10.1039/C7RA03144K.

Borra, C.R., Blanpain, B., Pontikes, Y., Binnemans, K., Van Gerven, T., 2017. Recovery of Rare Earths and Major Metals from Bauxite Residue (Red Mud) by Alkali Roasting, Smelting, and Leaching. J. Sustain. Metall. 3, 393–404. https://doi.org/10.1007/s40831-016-0103-3.

Chakraborty, D., Ranganathan, S., Sinha, S.N., 2005. Investigations on the carbothermic reduction of chromite ores. Metall. Mater. Trans. B 36, 437–444. https://doi.org/10.1007/s11663-005-0034-z.

Cheng, J., Li, H.-Y., Chen, X.-M., Hai, D., Diao, J., Xie, B., 2022. Eco-friendly chromium recovery from hazardous chromium-containing vanadium extraction tailings via low-dosage roasting. Process Saf. Environ. Prot. 164, 818–826. https://doi.org/10.1016/j.psep.2022.06.065.
Cunat, P.-J., 2004. Alloying elements in stainless steel and other chromium containing alloys. Paris.
Dawson, N F; Edwards, R.I., 1986. Factors affecting the reduction rate of chromite, in: Proceedings of INFACON IV 4th International Ferro Alloys Congress. pp. 105–113.
Ding, Y.L., Warner, N.A., 1997a. Kinetics and mechanism of reduction of carbonchromite composite pellets. Ironmak. Steelmak. 24, 224–229.
Ding, Y.L., Warner, N.A., 1997b. Catalytic reduction of carbon-chromite composite pellets by lime. Thermochim Acta 292, 85–94.
Duong, H.V., Johnston, R.F., 2000. Kinetics of solid state silica fluxed reduction of chromite with coal. Ironmak. Steelmak. 27, 202–206.
Escudero-Castejon, L., Sanchez-Segado, S., Parirenyatwa, S., Jha, A., 2016. Formation of Chromium-Containing Molten Salt phase during Roasting of Chromite Ore with Sodium and Potassium Hydroxides. J. Manuf. Sci. Prod. 16. https://doi.org/10.1515/jmsp-2016-0023.
Escudero-Castejón, L., Taylor, J., Sánchez-Segado, S., Jha, A., 2021. A novel reductive alkali roasting of chromite ores for carcinogen-free Cr6+-ion extraction of chromium oxide (Cr2O3) – a clean route to chromium product manufacturing! J. Hazard. Mater. 403, 123589. https://doi.org/10.1016/j.jhazmat.2020.123589.
Fastmarkets, n.d. Industrial minerals: chrome and chromite [WWW Document]. URL https://www.fastmarkets.com/industrial-minerals/chrome-and-chromite (accessed 8.12.22).
Geveci, A., Topkaya, Y., Ayhan, E., 2002. Sulfuric acid leaching of Turkish chromite concentrate. Miner. Eng. 15, 885–888. https://doi.org/10.1016/S0892-6875(02)00159-0.
Ghambi, S., Sanchez-Segado, S., Chipakwe, V., Jha, A., 2021. An investigation on hydrofluoric (HF) acid-free extraction for niobium oxide (Nb2O5) and tantalum oxide (Ta2O5) from columbite/tantalite concentrates using alkali reductive roasting. Miner. Eng. 173, 107183. https://doi.org/10.1016/j.mineng.2021.107183.
Ginstling, A.M., Brounshtein, B.I., 1950. Concerning the diffusion kinetics of reactions in spherical particles. J. Appl. Chem. USSR 23, 1327–1338.
Hazar-Yoruç, A.B., 2007. Reduction mechanism of chromite spinel with carbon. Mining. Metall. Explor. 24, 115–120. https://doi.org/10.1007/BF03403367.
Holappa, L., 2014. Iron and Steel Technology, in: Treatise on Process Metallurgy. Elsevier, p. 1. https://doi.org/10.1016/B978-0-08-096988-6.00001-8.
Jha, A., 2011. The alkali roasting of complex oxide minerals for high purity chemicals-beyond the Le Chatelier era into the 21st century. JOM 63, 39–42. https://doi.org/10.1007/s11837-011-0010-9.
Kekkonen, M., Xiao, Y., Holappa, L., 1995. Kinetic study on solid state reduction of chromite pellets. INFACON 7, 351–360.
Kundrat, D.M., Chochol, M., Elliott, J.F., 1984. Phase relationships in the Fe-Cr-C system at solidification temperatures. Metall. Trans. B 15, 663–676. https://doi.org/10.1007/BF02657287.
Lahiri, A., Jha, A., 2007. Kinetics and Reaction Mechanism of Soda Ash Roasting of Ilmenite Ore for the Extraction of Titanium Dioxide. Metall. Mater. Trans. B 38, 939–948. https://doi.org/10.1007/s11663-007-9095-5.
Mineral commodity summaries 2024, 2024. https://doi.org/10.3133/mcs2024.
Murti, N.S.S., Seshadri, V., 1982. Kinetics of reduction of synthetic chromite with carbon. Trans. Iron Steel Inst. Japan 22, 925–933.
Niayesh, MJ., Dippenaar, R.J., 1992. The solid-state reduction of chromite, in: Proceedings of INFACON VI 6th International Ferro Alloys Congress. pp. 57–63.
Nickens, K.P., Patierno, S.R., Ceryak, S., 2010. Chromium genotoxicity: a double-edged sword. Chem. Biol. Interact. 188, 276–288. https://doi.org/10.1016/j.cbi.2010.04.018.
Paktunc, D., Coumans, J.P., Carter, D., Zagrtdenov, N., Duguay, D., 2024. Mechanism of the Direct Reduction of Chromite Process as a Clean Ferrochrome Technology. ACS Eng. Au 4, 125–138. https://doi.org/10.1021/acsengineeringau.3c00057.
Papp, J.F., 1994. Chromium Life Cycle Study.
Parirenyatwa, S., Escudero-Castejon, L., Sanchez-Segado, S., Hara, Y., Jha, A., 2016. Comparative study of alkali roasting and leaching of chromite ores and titaniferous minerals. Hydrometall. 165, 213–226. https://doi.org/10.1016/j.hydromet.2015.08.002.
Ramakrishna, G., Kadrolkar, A., Srikakulapu, N.G., 2015. Exergy and its Efficiency Calculations in Ferrochrome Production. Metall. Mater. Trans. B 46, 1073–1081. https://doi.org/10.1007/s11663-014-0261-2.
Ranganathan, S., Godiwalla, K.M., Chakraborty, D., 2011. Investigation of the kinetics of reduction of chromite ore lumps with large particles of coke. Miner. Process. Extr. Metall. 120, 71–78. https://doi.org/10.1179/037195510X12816242170690.
Rao, Y.K., 1983. Catalysis in Extractive Metallurgy. JOM 35, 46–50. https://doi.org/10.1007/BF03338324.
Roine, A., 2002. HSC Chemistry 5.1.
Sanchez-Segado, S., Lahiri, A., Jha, A., 2014. Alkali roasting of bomar ilmenite: rare earths recovery and physico-chemical changes. Open Chem. 13. https://doi.org/10.1515/chem-2015-0033.
Sanchez-Segado, S., Makanyire, T., Escudero-Castejon, L., Hara, Y., Jha, A., 2015a. Reclamation of reactive metal oxides from complex minerals using alkali roasting and leaching – an improved approach to process engineering. Green Chem. 17, 2059–2080. https://doi.org/10.1039/C4GC02360A.
Sanchez-Segado, S., Monti, T., Katrib, J., Kingman, S., Dodds, C., Jha, A., 2017. Towards sustainable processing of columbite group minerals: elucidating the relation between dielectric properties and physico-chemical transformations in the mineral phase. Sci. Rep. 7, 18016. https://doi.org/10.1038/s41598-017-18272-3.
Sanchez-Segado, Sergio, Ruzaidi, A.F., Zhang, Y., Jha, A., 2015. Characterization of Physico-Chemical Changes during the Alkali Roasting of Niobium and Tantalum Oxides, in: Drying, Roasting, and Calcining of Minerals. Springer International Publishing, Cham, pp. 51–58. https://doi.org/10.1007/978-3-319-48245-3_7.
Sanchez-Segado, S., Stodd, S., Chipakwe, V., Loye, E., Smith, M., Wall, F., Abbott, A.P., Jha, A., 2022. Influence of the Alkali-promoted phase transformation in monazite for selective recovery of rare-oxides using deep eutectic solvents. Miner. Eng. 182, 107564. https://doi.org/10.1016/j.mineng.2022.107564.
Spencer, Wilfred Devonshire; Topley, B., 1929. Chemical kinetics of the system Ag2CO3⇌ Ag2O+ CO2. J. Chem. Soc. 2633–2650.
Statista, n.d. Global stainless steel production from 2010 to 2020 [WWW Document]. URL https://www.statista.com/statistics/223028/world-stainless-steel-production/#:~:text=In 2020%2C global stainless steel,under 50.9 million metric tons. (accessed 8.12.22).
Sun, Z., Zheng, S., Xu, H., Zhang, Y., 2007. Oxidation decomposition of chromite ore in molten potassium hydroxide. Int. J. Miner. Process. 83, 60–67. https://doi.org/10.1016/j.minpro.2007.04.005.
Tathavadkar, V.D., Jha, A., Antony, M.P., 2003. The effect of salt-phase composition on the rate of soda-ash roasting of chromite ores. Metall. Mater. Trans. B 34, 555–563. https://doi.org/10.1007/s11663-003-0024-y.
Tathavadkar, V.D., Jha, A., Antony, M.P., 2001. The soda-ash roasting of chromite minerals: Kinetics considerations. Metall. Mater. Trans. B 32, 593–602. https://doi.org/10.1007/s11663-001-0115-6.
Tathavakar, V.D., Antony, M.P., Jha, A., 2005. The physical chemistry of thermal decomposition of south african chromite minerals. Metall. Mater. Trans. B 36, 75–84. https://doi.org/10.1007/s11663-005-0008-1.
Thompson, S; Lawson, F., 1984. Chromite for the production of chromium chemicals, in: Proceedings of the Australian Institute of Mining and Metallurgy. pp. 113–116.
Tian, C., Lu, C., Yang, J., Xu, R., Zhang, M., Wen, J., Wang, Y., Zhang, S., He, Y., Luo, D., Luo, H., Zhang, X., 2025. An effective strategy for high-value utilization of chromite ore processing residue (COPR) through reductive alkali roasting and physical separation. Process Saf. Environ. Prot. 193, 874–885. https://doi.org/10.1016/j.psep.2024.11.103.
Tian, Y., Quan, X., Li, G., Tang, X., Qin, X., Wu, H., Zeng, K., Jiang, Z., 2022. A cleaner method for preparation of chromium oxide from chromite ore. Process Saf. Environ. Prot. 158, 87–97. https://doi.org/10.1016/j.psep.2021.11.052.
Tinjum, J.M., Benson, C.H., Edil, T.B., 2008. Mobilization of Cr(VI) from chromite ore processing residue through acid treatment. Sci. Total Environ. 391, 13–25. https://doi.org/10.1016/j.scitotenv.2007.10.041.
von Bogdandy, L., Engell, H.-J., 1971. Results of Experimental Investigations of the Kinetics of Reduction, in: The Reduction of Iron Ores. Springer Berlin Heidelberg, Berlin, Heidelberg, pp. 105–202. https://doi.org/10.1007/978-3-662-10400-2_3.
Voorhees, P.W., 1985. The theory of Ostwald ripening. J. Stat. Phys. 38, 231–252. https://doi.org/10.1007/BF01017860.
Wang, Y., Wang, L., Yu, J., Chou, K.C., 2014. Kinetics of carbothermic reduction of synthetic chromite. J. Min. Metall. Sect. B Metall. 50, 15–21.
Xiao, Y., Reuter, M.A., Holappa, L., 2001. Kinetic modelling of chromite pellet reduction with CO gas under rising temperatures from 700 to 1520 C, in: Proceedings of the Ninth International Ferroalloys Congress and the Manganese 2001 Health Issues Symposium: INFACON.
Yildiz, K., Sengil, I.A., 2004. Investigation of efficient conditions for chromate production from chromite concentrate by alkali fusion. Scand. J. Metall. 33, 251–256. https://doi.org/10.1111/j.1600-0692.2004.00694.x.